Article

J. Biol. Regul. Homeost. Agents. 2024; 38(6): 4973–4986
https://doi.org/10.23812/j.biol.regul.homeost.agents.20243806.397

Regulating Mitochondrial Biogenesis via Pachymaran: A Novel Treatment Strategy for Diabetic Cardiomyopathy

Zixin Yang[1,*], Chen Li[2]

[1]School of Public Health, Harbin Medical University, 150076 Harbin, Heilongjiang, China
[2]Traditional Chinese and Western Medicine Department, Hegang People's Hospital, 154100 Hegang, Heilongjiang, China
*Correspondence: Yangzixin0708@163.com (Zixin Yang)
Submitted: 28 December 2023 Revised: 31 January 2024 Accepted: 5 March 2024 Published: 1 June 2024

Background: Diabetic cardiomyopathy (DCM) is a common complication among diabetic patients, yet its pathogenesis is not fully understood. Mitochondrial dysfunction and oxidative stress play important roles in the development of DCM. Pachymaran (PPS), a natural compound with various biological properties, has not been extensively investigated in DCM. This study aims to explore the role and mechanism of PPS in DCM.

Methods: DCM model mice were initially divided into control, DCM, and PPS treatment groups (50 mg/kg and 100 mg/kg). Subsequently, we evaluated the effects of PPS on DCM via myocardial histopathological analysis, cardiac function assessment, and mitochondrial function detection. In addition, Western blot and real-time quantitative PCR were used to study the regulatory effects of PPS on mitochondrial biogenesis and Sirtuin 3 (SIRT3).

Results: PPS treatment in DCM mice exhibited significant myocardial protection, evident from reduced myocardial fibrosis upon histopathological examination ($p < 0.05$). Furthermore, cardiac function assessment revealed a significant improvement in myocardial contractile function in the PPS treatment group ($p < 0.01$). Moreover, enhanced activity of mitochondrial respiratory chain complexes and ATP synthesis capacity was observed in the PPS treatment group ($p < 0.01$), indicating improved mitochondrial function. Further research revealed that PPS significantly increased the expression level of SIRT3 and promoted expression of key regulators of mitochondrial biogenesis ($p < 0.01$).

Conclusion: The results of this study indicate that PPS protects against DCM by activating mitochondrial biogenesis and SIRT3. PPS can inhibit myocardial fibrosis, enhance myocardial contractile function, and improve mitochondrial function. Additionally, PPS can regulate SIRT3 expression and promote mitochondrial biogenesis. Therefore, PPS may be a potential drug for DCM treatment, proposing a new strategy for DCM treatment.

Keywords: PPS; DCM; mitochondrial biogenesis; SIRT3; myocardial protection

Introduction

Diabetic cardiomyopathy (DCM) is a common complication in diabetic patients, and yet its pathogenesis is not fully understood [1,2]. The characteristics of DCM include myocardial fibrosis, myocardial cell apoptosis, and impaired cardiac function [3]. While some therapeutic methods are available to alleviate the symptoms of DCM, effective treatment options are still lacking [4,5].

Recent studies have demonstrated that mitochondrial dysfunction and oxidative stress play crucial roles in the development of DCM [6,7]. Mitochondria are primarily cellular energy production centers, and their dysfunction results in inadequate energy supply and increased oxidative stress, thereby damaging the structure and function of myocardial cells [8–10]. Sirtuin 3 (SIRT3), a mitochondrial protein deacetylase, has emerged as a key contributor in modulating mitochondrial function and cellular stress responses [11]. Mitochondrial function is regulated by various factors, including mitochondrial biogenesis and mitochondrial homeostasis, where SIRT3, as a mitochondrial protein deacetylase, is believed to play a crucial role in regulating mitochondrial biogenesis and maintaining mitochondrial function [12,13].

Pachymaran (PPS) is a Ganoderma polysaccharide, isolated from Poria cocos and modified by carboxymethylation with enhanced pharmacological effects and aqueous solubility. PPS has various biological properties, inducing antioxidant, anti-inflammatory, and anti-fibrotic effects [14–16]. However, the mechanism of action of PPS in DCM and its regulatory effects on mitochondrial biogenesis and SIRT3 have not been thoroughly investigated. Therefore, it is necessary to further study the potential therapeutic effects of PPS in DCM.

This study aims to explore the role and mechanism of PPS in DCM. Initially, a DCM mouse model was established to evaluate the effects of PPS on DCM via myocardial histopathological analysis, cardiac function assessment, and mitochondrial function detection. Subsequently, techniques such as Western blot and real-time quantitative

Journal of
BIOLOGICAL REGULATORS
and Homeostatic Agents

PCR were utilized to study the regulatory effects of PPS on mitochondrial biogenesis and SIRT3. This study's significance lies in further elucidating the mechanism of action of PPS in DCM, providing a new strategy for DCM treatment. By activating mitochondrial biogenesis and increasing SIRT3 expression, PPS can inhibit myocardial fibrosis, enhance myocardial contractile function, and improve mitochondrial function. PPS may become a potential drug for DCM treatment, offering a new therapeutic strategy for improving the cardiac health of diabetic patients.

Methods

DCM Animal Model

Forty clean-grade C57BL/6 male mice (MODEL ORGANISMS, Shanghai, China), aged eight weeks, were raised in a clean-grade environment. The 40 mice were randomly divided into the following four groups: control, DCM, DCM+PPS (50 mg/kg), and DCM+PPS (100 mg/kg), with 10 mice in each group.

To induce the DCM model, 8-week-old male C57BL/6 mice received intraperitoneal injections of Streptozotocin (STZ, Lot: S0130, Sigma, St. Louis, MO, USA) for 3 consecutive days at a dose of 60 mg/kg). The mice underwent a 12-hour fast before each intraperitoneal injection. After 2 weeks, fasting blood glucose was measured following an eight-hour fast. A blood glucose level of $\geq$11.1 mmol/L indicated successful diabetes induction. Mice that developed diabetes were fed a high-calorie diet for 12 weeks to establish the DCM model. The control group and DCM group were orally administered normal saline, while the DCM+PPS group received daily oral PPS supplementation Pachymaran (PPS): (Lot: SP8903, Solarbio Company, Beijing, China) (100 mg/kg) for 12 weeks following 2 weeks of STZ injection (Fig. 1A). The dosages of PPS and STZ required for the experiment were referenced from previous literature [6,7]. After the experiment, mouse cardiac contractile function was detected using a small animal ultrasound machine. Eight weeks after modeling, mice were sacrificed by CO_2 asphyxiation, and blood samples were collected from the abdominal aorta. Various biochemical indicators in the mice were measured using a fully automated biochemical analyzer (Lot: 7180, Clinical Analyzer, Hitachi, Tokyo, Japan). This study was approved by the Ethics Committee of Harbin Medical University (Certificate No. KY2022-115).

Cells and Reagents

The H9c2 (CRL-1446) cardiomyocyte cell line was purchased from the ATCC cell bank in the United States. Cells were cultured using DMEM/F12 (Lot: 11965092, Gibco™, Grand Island, NY, USA) containing 10% fetal bovine serum (Lot: A5669701, Gibco™, Grand Island, NY, USA).

Pachymaran (PPS): (Lot: SP8903, Solarbio Company, Beijing, China). Restriction endonucleases (Lot: 3159), T4 DNA ligase (Lot: 2011A), SYBR Premix Ex TaqTM II (Lot: RR390Q), and reverse transcription reagents (PrimeScriptTM RT reagent kit, Lot: RR037Q): all from Takara (Tokyo, Japan). Plasmid extraction and gel recovery reagent kits: (Lot: 12123, QIAGEN, Duesseldorf, Germany). Transfection reagent Lipofectamine 2000 and RNA extraction reagent trizol: (Lot: 15596018CN, Invitrogen, Carlsbad, CA, USA). RIP, SDS-PAGE gel preparation kits: (Lot: P0012AC, Beyotime, Beijing, China). PVDF membrane and protein detection reagents: (Lot: 08321S, Merck Millipore, Billerica, MA, USA). Nuclear respiratory factor 1 (NRF-1) and nuclear respiratory factor 2 (NRF-2) were detected through the Colorimetric Nrf2 Transcription Factor Assay Kit (Lot: ab207213, Abcam, Cambridge, MA, USA) and the Colorimetric Nrf2 Transcription Factor Assay Kit (Lot: ab207223, Abcam, Cambridge, MA, USA).

Cardiac Function Detection

On the day preceding the cardiac ultrasound examination, the mice's chests were shaved. Subsequently, they were anesthetized with inhaled isoflurane (Lot: 5372, Ambion, Austin, TX, USA) and placed on a constant temperature detection platform. Once the heart rate stabilized at 400–500 beats/min, the ultrasound probe was adjusted, and M-mode ultrasound detection was performed using the VisualSonics Vevo2100 high-resolution small animal ultrasound system (FUJIFILM VisualSonics, Toronto, Canada) along with the RMV707B high-frequency probe (Lot: A1425, Hy Test Ltd, Turku, Finland) specifically designed for mice. Left ventricular ejection fraction (LVEF), left ventricular fractional shortening (LVFS), and stroke volume were measured through the small animal ultrasound system.

Measurement of Body Weight and Carbohydrate Metabolism

Mice were weighed and subsequently sacrificed. Euthanasia of mice via intraperitoneal injection of pentobarbital sodium (3 mg/mL) (110 mg/kg). Hearts were rapidly removed, trimmed to remove major blood vessels, sectioned, and blotted. Atrial natriuretic peptide (ANP) was measured through Mouse ANP ELISA Kit (Lot: ab267800, Abcam, Cambridge, MA, USA), while Brain natriuretic peptide (BNP) was measured with the Mouse BNP ELISA Kit (Lot: EEL089, Invitrogen, Carlsbad, CA, USA). Insulin levels were measured using the Mouse Insulin ELISA Kit (Lot: ab277390, Abcam, Cambridge, MA, USA). Free Fatty Acids (NEFA/FFA) were measured using the Fluorometric Assay Kit (Lot: E-BC-F039, Elabscience, Wuhan, China). Mice blood glucose, total cholesterol (TC), and triglyceride (TG) levels were detected by a semi-automatic biochemical analyzer (Lot: LABOSPECT 008 AS, Hitachi, Tokyo, Japan). The Homeostatic Model Assessment of β-

cell function (HOMA-β), an index evaluating islet β-cell function, was calculated as follows: (20 $\times$ fasting insulin level) / (fasting glucose level – 3.5).

Pathological Histology

The mice's hearts were dissected and placed in sterile cell culture dishes. The hearts were pressed to expel blood and then washed with physiological saline. A 2 mm transverse cut was made at the apex of the heart, and the excised apex tissue was fixed in 4% paraformaldehyde solution (Lot: B1820, Beyotime, Beijing, China) for 48 hours. After fixation, the tissue was dehydrated in a gradient of ethanol (Lot: B1820, Beyotime, Beijing, China), made transparent, embedded in paraffin, and sectioned. The sections were hydrated, stained with H&E and Sirius Red staining reagents (Lot: C0105S, Beyotime, Beijing, China), and observed under a microscope (Lot: LX23, Olympus, Tokyo, Japan) to compare the pathological changes in the myocardial tissue among the different groups of mice.

Western Blot

Fifty micrograms of total protein were separated by SDS-PAGE gel electrophoresis and were subsequently transferred onto a PVDF membrane. The membrane was then blocked with 5% skim milk at 37 °C for 2 hours. Specific antibodies (all purchased from Abcam, Cambridge, MA, USA), including phosphorylated AMP-activated protein kinase (p-AMPK, s487, 1:400), AMP-activated protein kinase (AMPK, ab3759, 1:400), phosphorylated protein kinase B (p-AKT, ab38449, 1:400), protein kinase B (AKT, ab65786, 1:400), manganese superoxide dismutase (Mn-SOD antibody, ab13533, 1:400), and glyceraldehyde-3-phosphate dehydrogenase (GAPDH, ab9485, 1:1000), were incubated with the membrane for 24 hours. Subsequently, the corresponding HRP-linked secondary antibodies were incubated with the membrane at 37 °C for 1 hour. Protein bands on the membrane were visualized using ECL luminescent fluid (Lot: 1792, Merck Millipore, Billerica, MA, USA) and imaged using the Bio-Rad system (Lot: 12011319, Bio-Rad, Hercules, CA, USA). The expression of each protein was evaluated using glyceraldehyde-3-phosphate dehydrogenase (GAPDH) as an internal reference.

Quantitative Reverse Transcription-polymerase Chain Reaction (qRT-PCR)

Total RNA was isolated from the tissue using trizol reagent (Lot: 15596018CN, Invitrogen, Carlsbad, CA, USA), followed by reverse transcription to synthesize cDNA. The concentrations and purities of RNA and cDNA were determined using a spectrophotometer (Lot: 6300X, Thermo Fisher Scientific, Waltham, MA, USA). Primers were designed using Primer Premier software (Version 6.0, PrimerPremier, Toronto, Canada) and synthesized by Jikai Gene (Shanghai, China). The primer sequences were as follows: *GAPDH*: F: 5′-GGCACAGTCAAGGCTGAGAATG-3′ and R: 5′-ATGGTGGTGAAGACGCCAGTA-3′; peroxisome proliferator-activated receptor gamma coactivator 1-alpha *(PGC-1α)*: F: 5′-AAGTGGTGTAGCGACCAATCG-3′ and R: 5′- AATGAGGGCAATCCGTCTTCA-3′; mitochondrial transcription factor A *(TFAM)*: F: 5′-GAGCAGCTAACTCCAAGTCAG-3′ and R: 5′-GAGCCGAATCATCCTTTGCCT-3′. The relative expression levels of the target genes were quantified using the $2^{-\Delta\Delta Ct}$ method.

MitoTracker Red Staining for Mitochondrial Content

Cells in the logarithmic growth phase were seeded onto confocal culture dishes. Upon adhesion to the dish, the culture medium was removed, and the cells were washed once with phosphate buffered saline (PBS). MitoTracker, a mitochondrial fluorescent probe (Lot: C1048, Beyotime, Beijing, China), was added and incubated for 30 minutes under the corresponding experimental culture conditions, followed by three washes with phosphate buffered saline (PBS, P3813, Sigma, St. Louis, MO, USA). 4′,6-diamidino-2-phenylindole (DAPI, D9542, Sigma, St. Louis, MO, USA) staining was then added and incubated for 30 minutes, followed by another wash with PBS. Finally, the cells were observed and images were captured using a laser confocal microscope (Lot: BX63, Olympus, Tokyo, Japan). The experiment was repeated three times for validation.

Cardiomyocyte Culture

H9c2 cells were cultured in dulbecco's modified eagle medium (DMEM)/F12 (Lot: 11965092, Gibco™, Grand Island, NY, USA) high-glucose medium supplemented with 10% fetal bovine serum. The cells were seeded at a density of 1 $\times$ 10^9 in 25 cm^2 culture flasks and maintained at 37 °C in a 5% CO_2-humidified atmosphere. Passaging occurred every 2 days. Subsequent experiments were conducted when the cell density reached 80%. The cells were qualified by mycoplasma detection.

RNA Interference and in Vitro Transcribed Mrna of SIRT3

Chemically synthesized 25-nucleotide stealth RNAi duplex oligonucleotides were purchased from Invitrogen (Carlsbad, CA, USA). RNAi-negative control HiGC (Invitrogen, Carlsbad, CA, USA) was used as a control siRNA.

For the preparation and microinjection of in vitro-transcribed Mrna, plasmids containing Sirt3–green fluorescent protein was linearized and used as templates for *in vitro* transcription using the T7 Message Machine Kit (Lot: AM1344, Ambion, Austin, TX, USA). The sequence was synthesized by GeneChem (Shanghai, China). The sense strand is 5′-AATTCAGCTTCCCTGGCTCTAGC AGCACAGAAATGGAAGCGAGTCGACATATTGGC

Journal of
BIOLOGICAL REGULATORS
and Homeostatic Agents

TGTTGCTGACTGCTTCCATACTGA-3′, and the antisense strand is 5′-CTAACTTGTCGACTCTCCAGAAC GGTGTGCTGGTGCGCTGGGTTTTGTGAG-3′. Synthesized RNA was polyadenylated further using poly(A) polymerase (Lot: 0AS72, American Research Products, Grandville, MI, USA) and dissolved in 150 Mm KCl at a final concentration of ~100 ng/mL. Diluted RNA was filtered, heated at 90 °C for 1 minute, and cooled on ice. H9c2 cells were transfected with either SIRT3 siRNA or control siRNA mixed with the transfection reagent (Lot: 309872, eBioscience, San Diego, CA, USA); final concentration: 100 Nm.

Hematoxylin and Eosin (HE) Staining

After dehydration and embedding of heart tissue, it was cut into 4 μm sections, affixed to glass slides, and placed in a 42 °C oven overnight. Subsequently, the sections were placed in an oven and baked at 60 °C for 1 hour. Deparaffinization and rehydration were performed using an alcohol gradient. After deparaffinization, the sections were soaked in distilled water and gently shaken for 4 minutes on a shaker bed to remove the alcohol. Hematoxylin staining (Lot: 7901, Beyotime, Beijing, China) of cell nuclei was performed by staining with hematoxylin solution for 2 minutes, followed by rinsing with running water for 6 minutes. After differentiation with 1% hydrochloric acid alcohol (C0161S, Beyotime, Shanghai, China), eosin staining was performed for 3 minutes, followed by for a 6-minute rinse with running water. Sections were dehydrated and sealed by sequentially placing the sections in 70%, 80%, 95% ethanol solutions, absolute ethanol, a 1:1 mixture of ethanol and xylene (Lot: 6462, Beyotime, Beijing, China), and absolute xylene. The sections were then air-dried and sealed with a neutral gum. Images were obtained using microscope (Lot: CX23, Olympus, Tokyo, Japan).

Sirius Red Staining of Collagen

Collagen fibers in heart sections were visualized with Sirius Red stain (Lot: 9549, Beyotime, Beijing, China). Paraffin-embedded fetal heart sections (5 μm) were deparaffinized, rehydrated, and stained in 0.1% Sirius Red in saturated picric acid for 1 h. Sections were rinsed twice with 0.5% acetic acid for 5 minutes each, dehydrated in three changes of 100% ethanol for 5 minutes each, and coverslipped for imaging using bright-field microscopy (Lot: CX23, Olympus, Tokyo, Japan).

Immunofluorescence Staining for SIRT3 Expression

Cells were grown on culture plates and washed with PBS three times. The cells were fixed with 4% paraformaldehyde (Lot: B1820, Beyotime, Beijing, China) at room temperature for 30 minutes, permeabilized with 0.2% Triton X-100 (Lot: B91230, Beyotime, Beijing, China) at room temperature for 20 minutes, and then washed with PBS three times for 5 minutes each. Subsequently, the cells were blocked with 5% goat serum (Lot: 5532, Beyotime, Beijing, China) at room temperature for 60 minutes. After removing the blocking solution, the cells were incubated with the primary antibody (SIRT3, 1:100, Lot: ab217319, Abcam, Cambridge, MA, USA) at 4 °C overnight. The cells were subsequently washed four times with PBST (PBS+0.05% Tween20, Lot: BL314B, biosharp, Beijing, China) for 5 minutes each and then incubated with a diluted fluorescent-labeled secondary antibody in the dark at room temperature for 2 hours. After removing excess liquid, 50 mL of DAPI-containing anti-fade mounting medium was added to each slide. The cells were observed and images were captured using a fluorescence microscope (Lot: CX23, Olympus, Tokyo, Japan).

TUNEL Staining

Terminal deoxynucleotidyl transferase dutp nick-end labeling (TUNEL assay kit, Lot: C1091, Beyotime, Beijing, China) was used to detect apoptosis in cardiomyocytes. Cells were stained with TUNEL working solution, washed with PBS, and then stained with DAPI to label the cell nuclei. After fixing the cells with an anti-fade mounting medium, they were air-dried at room temperature and observed under a fluorescence microscope to assess cardiomyocyte apoptosis. The TUNEL-positive cells, indicating apoptotic cells, were marked by green fluorescence, while the cell nuclei were marked by blue fluorescence. Cell counting was performed in six random fields, and the ratio of TUNEL-positive cells to total cells was recorded as the TUNEL-positive cell ratio.

Statistical Analysis

Data obtained from the experiments were statistically analyzed using GraphPad Prism (Version 8.0; GraphPad Inc., La Jolla, CA, USA). Continuous data were presented as mean ± standard deviation. A one-way ANOVA is used to compare means across more than two groups, while differences between two groups were analyzed using *t*-tests. A significance level of $p < 0.05$ was considered statistically significant.

Results

The Therapeutic Effects of PPS on Mice with DCM

The experiment was conducted with 4 groups: Control, DCM, DCM+PPS (50 mg/kg), and DCM+PPS (100 mg/kg) (Fig. 1A). In the different treatment groups, mice treated with PPS 100 mg/kg showed similar body weight to the Control group ($p = 0.85$, Control vs. PPS 100 mg/kg), while those in the DCM group had the lowest body weight ($p < 0.01$, Control vs. DCM). This suggests that PPS may help maintain mouse body weight, with higher PPS dosages potentially being more effective (Fig. 1B). Blood glucose levels varied, with PPS demonstrating the ability to reduce blood glucose levels, an effect that became more

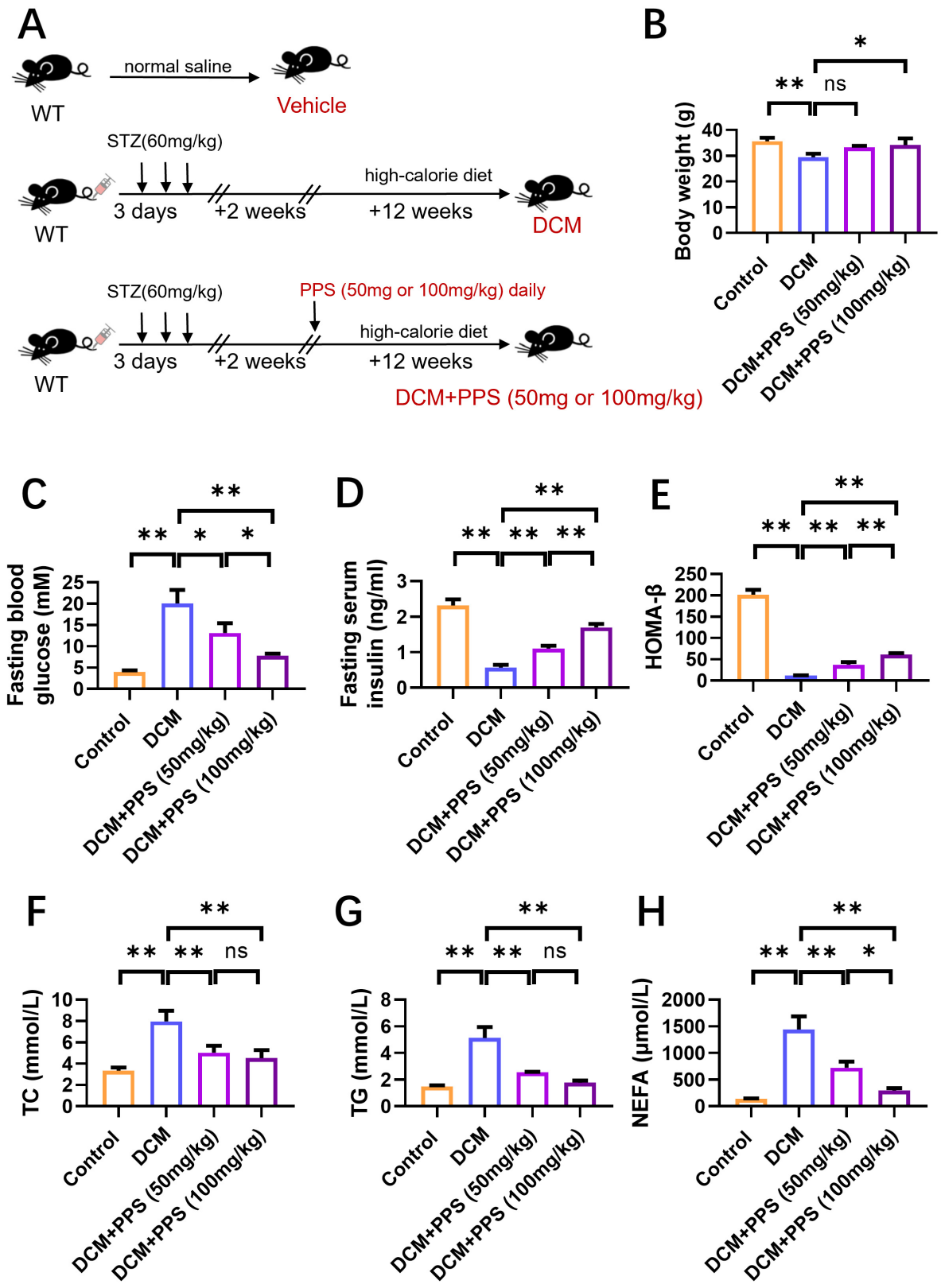

Fig. 1. Therapeutic effects of PPS on mice with diabetic cardiomyopathy (DCM). (A) Timeline of drug administration and DCM model. (B) Body weight of mice. (C) Fasting blood glucose levels (mM). (D) Fasting serum insulin levels (ng/mL). (E) Homeostasis model assessment-β cell function index, HOMA-β. (F) Total cholesterol, TC (mmol/L). (G) Triglycerides, TG (mmol/L). (H) Non-esterified fatty acid (NEFA) levels (μmol/L). n = 10 independent replicates. ns, no significance, *$p < 0.05$, **$p < 0.01$, PPS, pachymaran; WT, wild type mouse.

Journal of
BIOLOGICAL REGULATORS
and Homeostatic Agents

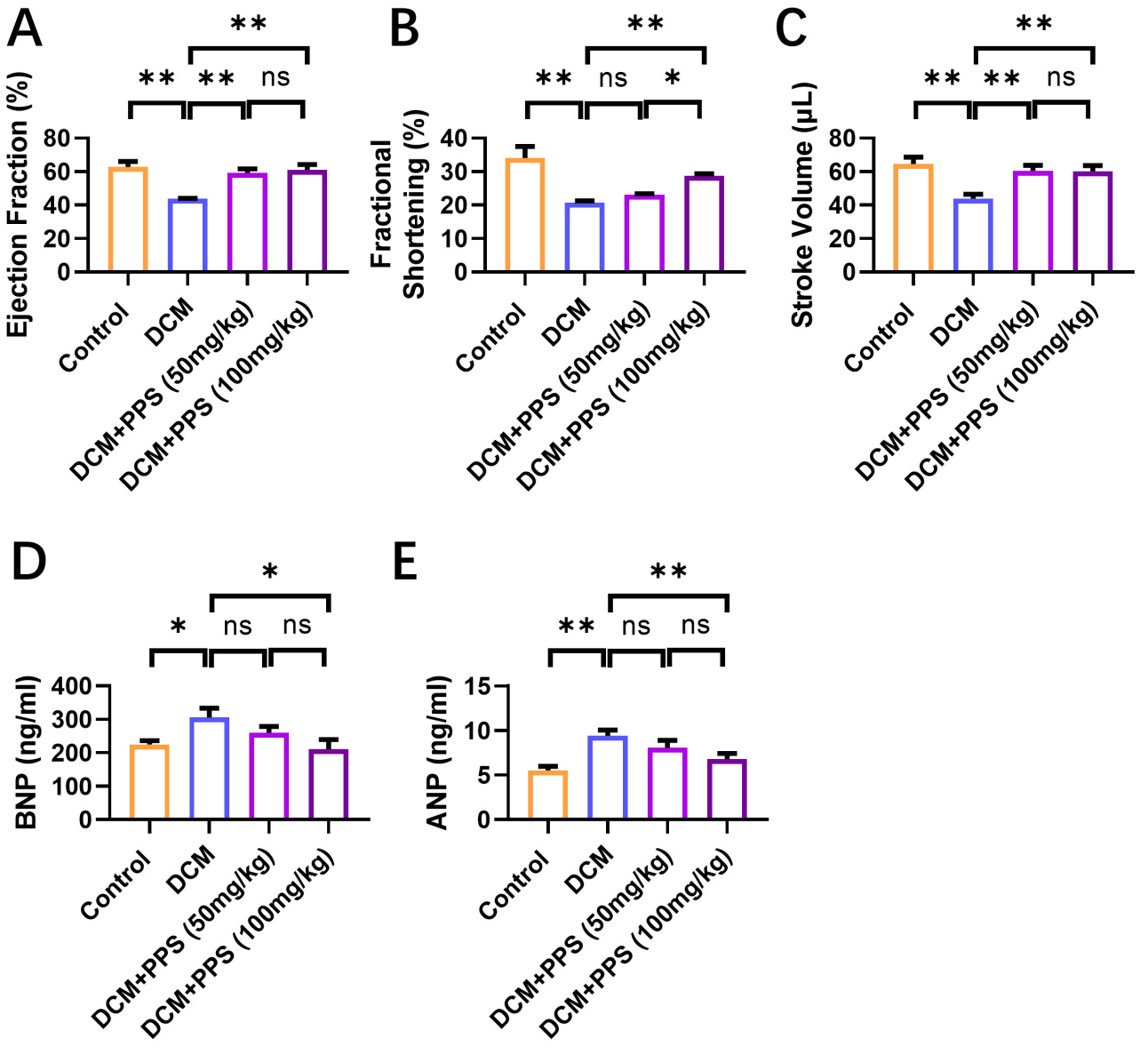

Fig. 2. Effects of PPS on cardiac function in DCM mice. (A) Left ventricular ejection fraction (LVEF). (B) Fractional shortening (FS). (C) Assessment of stroke volume. (D) Serum atrial natriuretic peptide (ANP) levels. (E) Brain natriuretic peptide (BNP) levels. n = 10 independent replicates. ns, no significance, *$p < 0.05$, **$p < 0.01$.

pronounced at higher dosages ($p < 0.01$) (Fig. 1C). The Control group had the highest serum insulin levels (2.32 ± 0.21 ng/mL), followed by the DCM+PPS (100 mg/kg) group (1.80 ± 0.13 ng/mL), then the DCM+PPS (50 mg/kg) group (0.68 ± 0.11 ng/mL), and lastly the DCM group (0.71 ± 0.12 ng/mL). This indicates that PPS may protect against DCM by affecting insulin levels (Fig. 1D). HOMA-β serves as an indicator of pancreatic function, with higher values suggesting better pancreatic function. The Control group exhibited the highest HOMA-β levels, followed by the DCM+PPS (100 mg/kg) group, in comparison, the DCM group had the lowest HOMA-β levels ($p < 0.01$), implying that PPS may protect against DCM by improving pancreatic function (Fig. 1E). Total cholesterol (TC) (Fig. 1F) and triglycerides (TG) (Fig. 1G) exhibited similar trends, with the Control group having the lowest levels, followed by the DCM+PPS (100 mg/kg) and DCM+PPS (50 mg/kg) groups, while the DCM group exhibited the highest levels ($p < 0.01$). This suggests a potential protective role of PPS in cardiovascular health. Non-esterified fatty acid (NEFA) levels, indicative of fatty acid metabolism, are crucial for lipid metabolism assessment. In this study, the NEFA levels exhibited a similar trend to TC and TG, indicating that PPS may protect against DCM by regulating lipid metabolism (Fig. 1H). Thus, PPS treatment improved the metabolic parameters of DCM mice, especially at the higher dose.

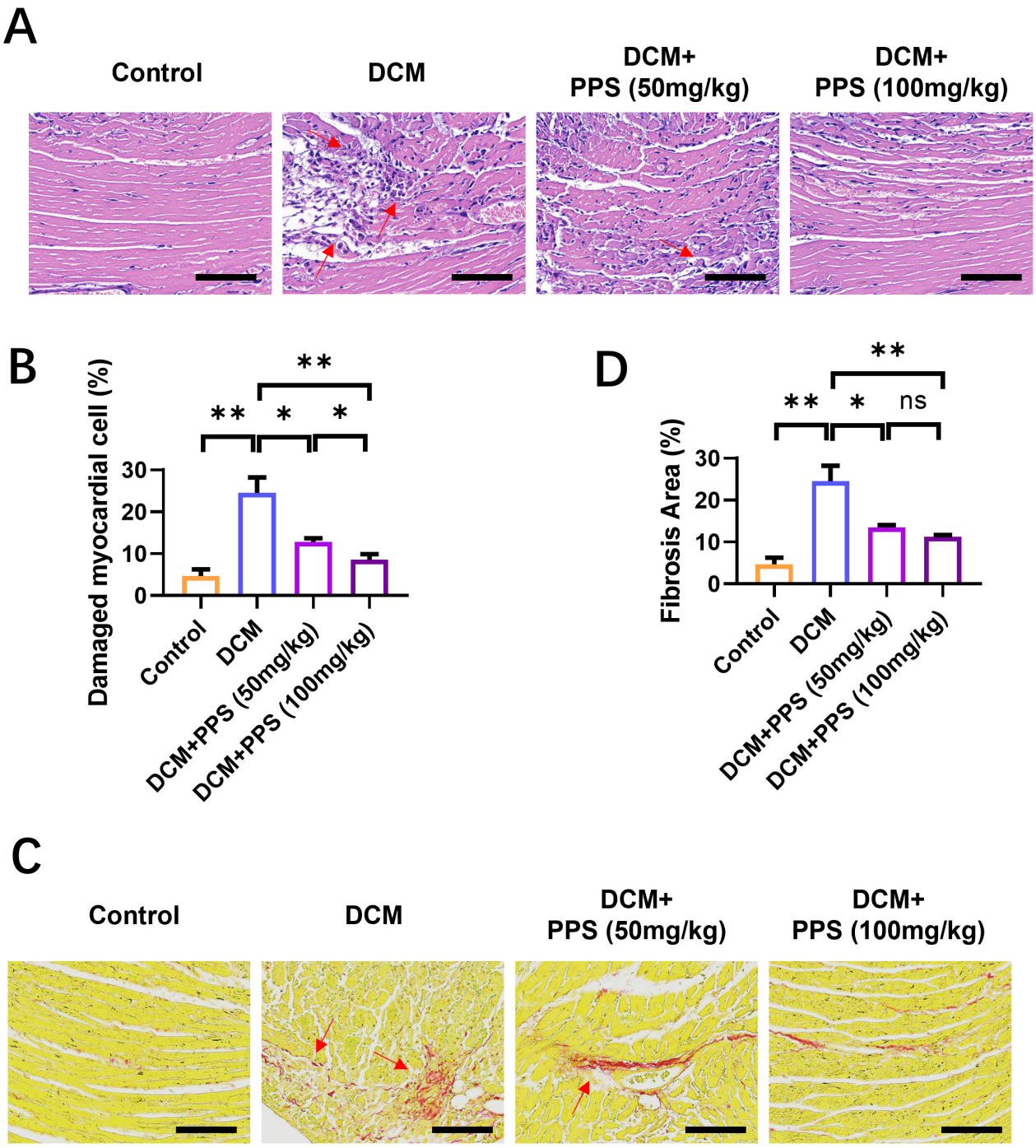

Fig. 3. Effects of PPS on the pathological morphology of myocardial tissue in DCM mice. (A) Evaluation of myocardial cell damage by hematoxylin and eosin (HE) staining. Red arrows represent areas of tissue damage. Scale bar = 100 μm. (B) Assessment of damaged myocardial cells. (C) Assessment of fibrotic area by Masson's trichrome staining. The arrows indicate collagen fibers. Scale bar = 100 μm. (D) Assessment of fibrosis area. n = 10 independent replicates. ns, no significance, *$p < 0.05$, **$p < 0.01$.

Effects of PPS on Cardiac Function in Mice with DCM

The left ventricular ejection fraction (LVEF), a crucial indicator of cardiac pumping function, with higher values reflecting better cardiac pumping function. It exhibited the highest values in the PPS 100 mg/kg group (61.5 ± 2.4%), followed by the Control group (58.1 ± 2.2%) and the PPS 50 mg/kg group (57.8 ± 3.2%), with the lowest LVEF observed in the DCM group (40.1 ± 1.1%). This indicates a significant enhancement in cardiac pumping function with PPS treatment, particularly at higher doses (Fig. 2A). Fractional shortening (FS) is another indicator of cardiac con-

Journal of
BIOLOGICAL REGULATORS
and Homeostatic Agents

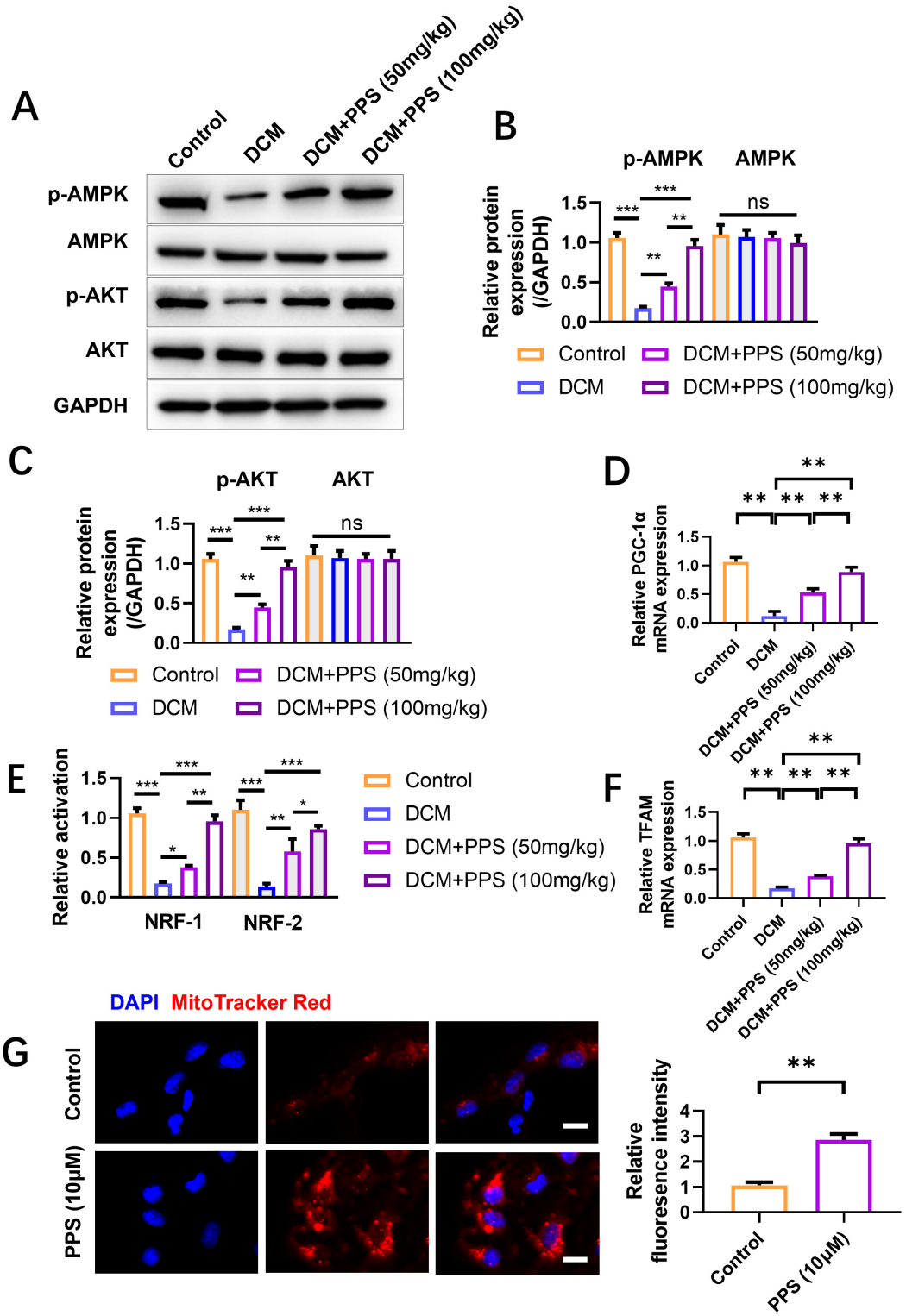

Fig. 4. PPS activates AMPK to upregulate Akt phosphorylation and the expression of PGC-1α and TFAM, enhancing mitochondrial function. (A) Measurement of AMPK and Akt phosphorylation levels. (B) Quantification of AMPK and AMPK phosphorylation levels. (C) Quantification of Akt and Akt phosphorylation levels. (D) qRT-PCR detection of PGC-1α expression. (E) Reactive activation of NRF-1 and NRF-2. (F) qRT-PCR detection of TFAM expression. (G) Treatment of cardiomyocytes with PPS (10 μM) for 3 hours. Mitochondrial content identified by MitoTracker Red staining. Scale bar = 10 μm. n = 10 independent replicates. ns, no significance, *$p < 0.05$, **$p < 0.01$, ***$p < 0.001$. NRF, nuclear respiratory factor; AMPK, AMP-activated protein kinase; Akt, protein kinase B; PGC-1α, peroxisome proliferator-activated receptor gamma coactivator 1-alpha; TFAM, mitochondrial transcription factor A; qRT-PCR, quantitative reverse transcription-polymerase chain reaction; GAPDH, glyceraldehyde 3-phosphate dehydrogenase.

tractile function, with higher values indicating better cardiac contractile function. PPS treatment improved cardiac contractile function in mice, with a significantly effect at higher doses ($p < 0.01$) (Fig. 2B). Stroke volume, indicative of cardiac pumping efficiency, was notably enhanced with PPS treatment in mice ($p < 0.01$) (Fig. 2C). Atrial natriuretic peptide (ANP) and brain natriuretic peptide (BNP) levels, markers of cardiac dysfunction, were lowest in the Control group, followed by the PPS 100 mg/kg group, the PPS 50 mg/kg group, and highest in the DCM group. This suggests PPS's protective effect on cardiac function, mitigating the release of these markers (Fig. 2D,E).

Effects of PPS on the Pathological Morphology of Myocardial Tissue in DCM Mice

HE staining was used to evaluate myocardial cell damage. Compared to the Control group, the DCM group exhibited severe morphological changes indicating myocardial injury, including vacuolization, myofibrillar disarray, cytoplasmic granulation, inflammatory infiltration, and fibrosis. Conversely, both the PPS 100 mg/kg ($p < 0.01$) and PPS 50 mg/kg ($p < 0.05$) treatment groups showed a protective effect against myocardial damage, with the higher dose showing a more significant effect (Fig. 3A,B). Sirius Red staining was used to evaluate the fibrotic area. The Control group had the smallest fibrotic area, followed by the PPS 100 mg/kg and PPS 50 mg/kg groups, while the DCM group had the largest fibrotic area (Fig. 3C,D). These findings also indicate that PPS can significantly reduce myocardial fibrosis in DCM mice, with higher doses of PPS showing a more significant effect.

PPS Upregulates the Expression of Akt Phosphorylation, PGC-1α, and TFAM by Activating AMPK, thus Increasing Mitochondrial Function

The experimental results in Fig. 4A–C demonstrate that the phosphorylation levels of p-AMPK and p-AKT were significantly higher ($p < 0.001$) in the PPS treatment groups compared to the DCM group, with a more pronounced effect observed at higher PPS doses. This indicates that PPS can increase intracellular metabolic activity and antioxidant capacity by activating AMPK and upregulating Akt phosphorylation levels. Additionally, qRT-PCR analysis demonstrated markedly increased expression levels of PGC-1α ($p < 0.01$) (Fig. 4D) and TFAM ($p < 0.01$) (Fig. 4F) in the PPS treatment groups compared to the DCM group, with the higher PPS dose exhibiting a more significant effect. Meanwhile, NRF-1 and NRF-2 are indispensable redox-determining factors essential for maintaining mitochondrial homeostasis by integrating multi-hierarchical regulatory networks. In our study, we assessed the reactive activation of NRF-1 and NRF-2, revealing significantly higher levels in the PPS treatment groups compared to the DCM group ($p < 0.05$), particularly with the higher PPS dose ($p < 0.01$) (Fig. 4E). This indicates that PPS can upregulate the expression of PGC-1α, NRF-1, NRF-2, and TFAM, thereby promoting mitochondrial biogenesis and function (Fig. 4F). Myocardial cell lines were treated with PPS (10 μM) for 3 hours. MitoTracker Red staining was used to identify mitochondrial content. The experimental results demonstrated significantly higher mitochondrial content in the PPS treatment group compared to the Control group ($p < 0.01$), suggesting the potential of PPS to improve mitochondrial function (Fig. 4G).

PPS Activates SIRT3

Measurement of SIRT3 levels (Fig. 5A) demonstrated significantly lower levels in the DCM group compared to the Control group ($p < 0.01$). However, SIRT3 levels in the PPS treatment group are comparable to those in the Control group, indicating that PPS can upregulate SIRT3 levels in DCM. Immunofluorescence staining was used to determine the expression of SIRT3 in myocardial cell lines treated with PPS (10 μM) for 3 hours. The results demonstrate a significant increase in SIRT3 expression in the PPS treatment group compared to the Control group ($p < 0.01$). This indicates that PPS can significantly increase SIRT3 expression (Fig. 5B).

The Effect of PPS on MnSOD Activity and Cell Apoptosis

Manganese superoxide dismutase (MnSOD) is an important antioxidant enzyme primarily found in the mitochondria, functioning to eliminate superoxide anions in the mitochondria, thus reducing oxidative damage. To elucidate the molecular mechanisms of diabetic cardiomyopathy mediated by PPS, we selected H92C cardiomyocytes and added normal saline (control) or high glucose (HG, 33.3 mM) during cultivation to simulate a diabetic high glucose environment. The use of mannitol serves the purpose of being an isotonic control group. Mannitol, being an inert substance with similar osmotic properties to the active substances being tested, helps maintain isotonic conditions in the experimental setup. Using mannitol as a control ensures that any observed effects are attributable to the treatment substances rather than osmotic variations. These results reveal significantly higher expression levels of MnSOD in the PPS treatment group compared to the HG-induced group ($p < 0.01$). This indicates that PPS can significantly increase MnSOD expression, thereby facilitating the clearance of mitochondrial reactive oxygen species (ROS) and mitigating oxidative stress damage (Fig. 6A). Under HG-induced conditions, the level of cell apoptosis was determined by TUNEL staining, demonstrating similarly reduced levels in the HG+siRNA NC+PPS group and the HG+PPS compared to the HG group. However, after silencing SIRT3, the protective effect of PPS on apoptosis disappears ($p < 0.01$) (Fig. 6B). These results demonstrated that PPS protects against high glucose-induced cardiomyocyte apoptosis by activating SIRT3.

Journal of
BIOLOGICAL REGULATORS
and Homeostatic Agents

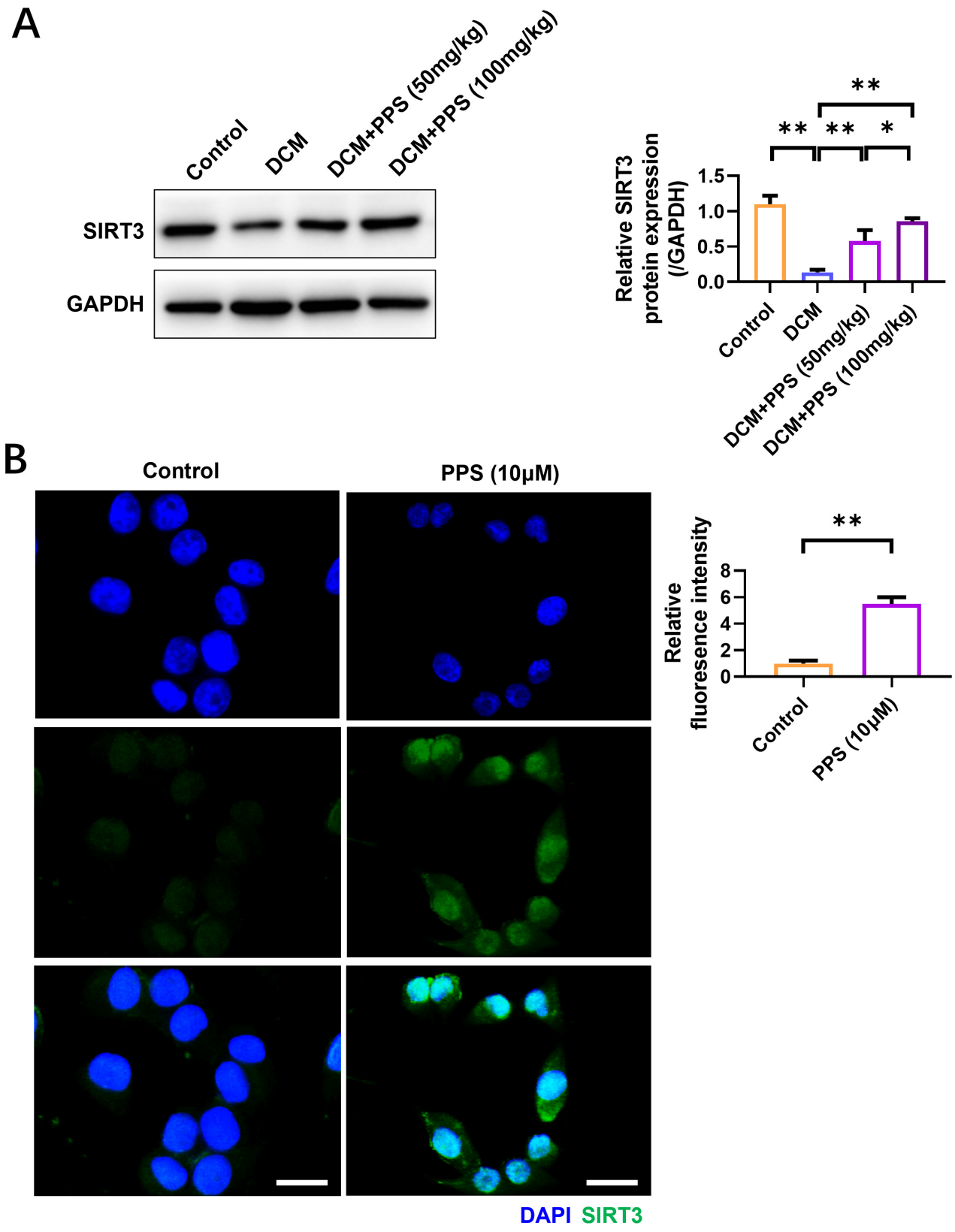

Fig. 5. Activation of SIRT3 by PPS. (A) Measurement of SIRT3 levels. (B) Immunofluorescence staining to determine SIRT3 expression after cardiomyocyte treatment with PPS (10 μM) for 3 hours. Scale bar = 10 μm. n = 10 independent replicates. *$p < 0.05$, **$p < 0.01$. SIRT3, Sirtuin 3; DAPI, 4',6-diamidino-2-phenylindole.

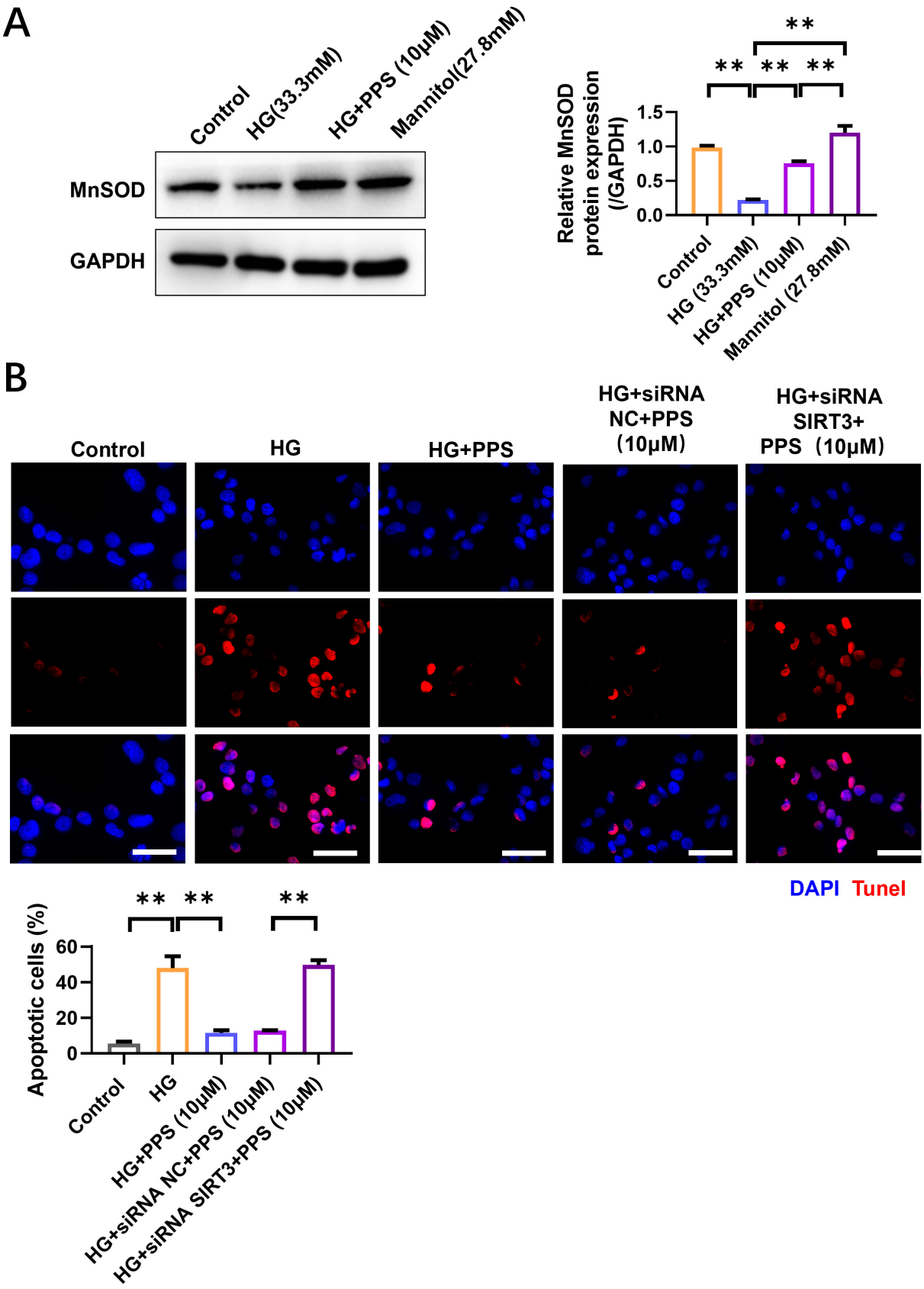

Fig. 6. Effects of PPS on MnSOD activity and mitochondrial ROS. (A) Measurement of MnSOD expression. (B) Assessment of cell apoptosis. Scale bar = 50 μm. n = 10 independent replicates. $^{**}p < 0.01$. MnSOD, manganese superoxide dismutase; ROS, reactive oxygen species; HG, high glucose.

Journal of
BIOLOGICAL REGULATORS
and Homeostatic Agents

Discussion

This study aimed to investigate the protective effects of PPS, a Ganoderma polysaccharide, in DCM and explore its relationship with mitochondrial biogenesis and SIRT3. Our findings demonstrate that PPS can protect the heart from DCM by activating mitochondrial biogenesis and SIRT3. Additionally, PPS reduces myocardial oxidative stress levels in DCM patients, thereby decreasing oxidative damage, myocardial cell apoptosis, and fibrosis.

Mitochondria are essential organelles in myocardial cells, and their dysfunction is closely associated with the onset and progression of DCM [17–19]. The results from this study indicate that PPS treatment can maintain normal mitochondrial function. SIRT3, an important mitochondrial deacetylase, contributes to the regulation of mitochondrial function and maintenance of energy metabolism balance. Our study reveals that PPS treatment significantly increases the expression and activity of SIRT3. Upregulation of SIRT3 may improve mitochondrial function by inhibiting mitochondrial ROS production. Furthermore, PPS activates the AMPK signaling pathway, further enhancing mitochondrial function. Therefore, by activating SIRT3 to protect mitochondrial function, PPS exhibits therapeutic potential for DCM.

As a natural medicine, PPS demonstrates good safety and tolerance [20]. Researches have indicated the absence of notable toxic side effects associated with PPS treatment in DCM [21,22]. Moreover, PPS exhibits antioxidant and anti-inflammatory effects capable of alleviating myocardial damage and inflammatory responses [15,23]. Therefore, PPS holds potential clinical value as a novel therapeutic agent for DCM. The results of this study align with existing literature [21,22], suggesting that the activation of mitochondrial biogenesis can alleviate myocardial damage. Additionally, study has shown that SIRT3 activation can improve cardiac function and reduce myocardial cell apoptosis [24]. Reducing myocardial oxidative stress levels can decrease cardiac injury [25]. This study holds significant academic and clinical implications for the treatment and cardiac protection strategies for DCM. By revealing the mechanisms through which PPS activates mitochondrial biogenesis and SIRT3, this study not only deepens the understanding of cardiac protection but also provides important guidance for developing additional cardiac protection strategies and drugs. The results of this study offer new insights and strategies for the treatment of DCM, making a significant contribution to improving patients' quality of life and prognosis.

In discussing the entry of PPS into the mitochondria and its interaction with SIRT3, it is essential to delve into the underlying mechanisms. PPS can enter the mitochondria through passive diffusion due to its physicochemical properties, such as molecular size and lipophilicity [14–16]. Alternatively, PPS can be actively transported into the mitochondria via specific transporters or channels present in the mitochondrial membrane [20]. Once inside the mitochondria, PPS may localize to the mitochondrial matrix where it can interact with various mitochondrial proteins, including SIRT3.

SIRT3 is a member of the sirtuin family of nicotinamide adenine dinucleotide (NAD+)-dependent deacetylases, primarily localized within the mitochondria [24]. SIRT3 plays a critical role in regulating mitochondrial functions by deacetylating specific protein targets. The interaction between PPS and SIRT3 may involve the modulation of specific signaling pathways or gene expression patterns that are regulated by SIRT3. PPS may enhance the deacetylase activity of SIRT3, leading to the deacetylation of key mitochondrial proteins involved in energy metabolism and oxidative stress defense. Through its interaction with SIRT3, PPS may promote mitochondrial health and function, potentially offering protective effects. PPS likely exerts its biological effects through a complex interplay of pathways involving AMPK activation, modulation of Akt signaling, and regulation of key mitochondrial regulators like PGC-1α and TFAM. Furthermore, PPS's impact on MnSOD activity and mitochondrial ROS production underscores its potential implications for mitochondrial function and oxidative stress modulation. These interactions may promote mitochondrial biogenesis, oxidative stress response, and energy metabolism.

Further research is warranted to elucidate the precise mechanisms governing the interplay between PPS and SIRT3, potentially paving the way for tailored structural modifications of PPS to optimize mitochondrial targeting efficiency and bioavailability. Harnessing the therapeutic potential of PPS through preclinical and clinical studies could shed light on dose optimization, treatment duration, and safety profiles, offering novel strategies to address mitochondrial dysfunction and associated disorders. While the results of this study suggest the potential of PPS as a new strategy for treating DCM, several unresolved issues warrant further investigation. Firstly, the efficacy and safety of PPS in humans remain unconfirmed, as this study utilized animal models, highlighting the need for clinical trials. Secondly, the specific regulatory mechanisms of PPS on the AMPK signaling pathway, mitochondrial ROS production, and mitochondrial fusion and fission need further exploration. Additionally, it is worth investigating whether the combined use of PPS with other drugs for DCM treatment can produce a synergistic effect. Finally, further exploration is needed to understand the duration of the therapeutic effect and the dose-response relationship of PPS.

Conclusion

The results of this study demonstrate that PPS protects against DCM by activating mitochondrial biogenesis and SIRT3. As a natural medicine, PPS contributes to nu-

merous pharmacological activities and holds promise as a new strategy for DCM treatment. By regulating the mitochondrial fusion-fission balance, PPS protects mitochondrial function by activating SIRT3. With favorable safety and tolerance, PPS holds promise for long-term use. However, further research is needed to clarify the mechanisms of action, clinical efficacy, and safety of PPS to promote its clinical application.

Availability of Data and Materials

All experimental data included in this study can be obtained by contacting the corresponding author if needed.

Author Contributions

ZY performed the experiments, analyzed the data, and wrote the manuscript. CL proposed and designed the study, interpreted the results, wrote the manuscript, and oversaw the project. Both authors contributed to editorial changes in the manuscript. Both authors read and approved the final manuscript. Both authors have participated sufficiently in the work to take public responsibility for appropriate portions of the content and agreed to be accountable for all aspects of the work in ensuring that questions related to its accuracy or integrity.

Ethics Approval and Consent to Participate

This study was approved by the Ethics Committee of Harbin Medical University (Certificate No. KY2022-115).

Acknowledgment

Not applicable.

Funding

This research received no external funding.

Conflict of Interest

The authors declare no conflict of interest.

References

[1] Tan Y, Zhang Z, Zheng C, Wintergerst KA, Keller BB, Cai L. Mechanisms of diabetic cardiomyopathy and potential therapeutic strategies: preclinical and clinical evidence. Nature Reviews. Cardiology. 2020; 17: 585–607.

[2] Dillmann WH. Diabetic Cardiomyopathy. Circulation Research. 2019; 124: 1160–1162.

[3] Paolillo S, Marsico F, Prastaro M, Renga F, Esposito L, De Martino F, *et al*. Diabetic Cardiomyopathy: Definition, Diagnosis, and Therapeutic Implications. Heart Failure Clinics. 2019; 15: 341–347.

[4] Murtaza G, Virk HUH, Khalid M, Lavie CJ, Ventura H, Mukherjee D, *et al*. Diabetic cardiomyopathy - A comprehensive updated review. Progress in Cardiovascular Diseases. 2019; 62: 315–326.

[5] Ritchie RH, Abel ED. Basic Mechanisms of Diabetic Heart Disease. Circulation Research. 2020; 126: 1501–1525.

[6] Gollmer J, Zirlik A, Bugger H. Mitochondrial Mechanisms in Diabetic Cardiomyopathy. Diabetes & Metabolism Journal. 2020; 44: 33–53.

[7] Qi B, He L, Zhao Y, Zhang L, He Y, Li J, *et al*. Akap1 deficiency exacerbates diabetic cardiomyopathy in mice by NDUFS1-mediated mitochondrial dysfunction and apoptosis. Diabetologia. 2020; 63: 1072–1087.

[8] Wende AR, Schell JC, Ha CM, Pepin ME, Khalimonchuk O, Schwertz H, *et al*. Maintaining Myocardial Glucose Utilization in Diabetic Cardiomyopathy Accelerates Mitochondrial Dysfunction. Diabetes. 2020; 69: 2094–2111.

[9] Kaludercic N, Di Lisa F. Mitochondrial ROS Formation in the Pathogenesis of Diabetic Cardiomyopathy. Frontiers in Cardiovascular Medicine. 2020; 7: 12.

[10] Sygitowicz G, Sitkiewicz D. Mitochondrial Quality Control: the Role in Cardiac Injury. Frontiers in Bioscience (Landmark Edition). 2022; 27: 96.

[11] Bugga P, Alam MJ, Kumar R, Pal S, Chattopadyay N, Banerjee SK. Sirt3 ameliorates mitochondrial dysfunction and oxidative stress through regulating mitochondrial biogenesis and dynamics in cardiomyoblast. Cellular Signalling. 2022; 94: 110309.

[12] Wu J, Zeng Z, Zhang W, Deng Z, Wan Y, Zhang Y, *et al*. Emerging role of SIRT3 in mitochondrial dysfunction and cardiovascular diseases. Free Radical Research. 2019; 53: 139–149.

[13] Lee S, Jeon YM, Jo M, Kim HJ. Overexpression of SIRT3 Suppresses Oxidative Stress-induced Neurotoxicity and Mitochondrial Dysfunction in Dopaminergic Neuronal Cells. Experimental Neurobiology. 2021; 30: 341–355.

[14] Liu F, Zhang L, Feng X, Ibrahim SA, Huang W, Liu Y. Immunomodulatory Activity of Carboxymethyl Pachymaran on Immunosuppressed Mice Induced by Cyclophosphamide. Molecules (Basel, Switzerland). 2021; 26: 5733.

[15] Zhang Z, Yang Y, Hu C, Zhang Z. Effect of pachymaran on oxidative stress and DNA damage induced by formaldehyde. Scientific Reports. 2023; 13: 17465.

[16] Zhao Y, Feng X, Zhang L, Huang W, Liu Y. Antitumor Activity of Carboxymethyl Pachymaran with Different Molecular Weights Based on Immunomodulatory and Gut Microbiota. Nutrients. 2023; 15: 4527.

[17] Berthiaume JM, Kurdys JG, Muntean DM, Rosca MG. Mitochondrial NAD^+/NADH Redox State and Diabetic Cardiomyopathy. Antioxidants & Redox Signaling. 2019; 30: 375–398.

[18] Ma XM, Geng K, Law BYK, Wang P, Pu YL, Chen Q, *et al*. Lipotoxicity-induced mtDNA release promotes diabetic cardiomyopathy by activating the cGAS-STING pathway in obesity-related diabetes. Cell Biology and Toxicology. 2023; 39: 277–299.

[19] Mu J, Zhang D, Tian Y, Xie Z, Zou MH. BRD4 inhibition by JQ1 prevents high-fat diet-induced diabetic cardiomyopathy by activating PINK1/Parkin-mediated mitophagy in vivo. Journal of Molecular and Cellular Cardiology. 2020; 149: 1–14.

[20] Gao MJ, Liu LP, Li S, Lyu JL, Jiang Y, Zhu L, *et al*. Multistage glucose/pachymaran co-feeding enhanced endo-β-1,3-glucanase production by Trichoderma harzianum via simultaneous increases in cell concentration and inductive effect. Bioprocess and Biosystems Engineering. 2020; 43: 1479–1486.

[21] Zhou J, Ma X, Zhang G. Analysis of prescription rules in the treatment of diabetic heart disease based on traditional Chinese medicine inheritance support system. Drug Combination Therapy. 2019; 1: 199–209.

[22] Liu J, Deng W, Fan L, Tian L, Jin L, Jin Z, *et al*. The role of radix hedysari polysaccharide on the human umbilical vein endothe-

Journal of
BIOLOGICAL REGULATORS
and Homeostatic Agents

lial cells (HUVECs) induced by high glucose. European Journal of Internal Medicine. 2012; 23: 287–292.

[23] He J, Hu L, Deng Q, Sun L, Zhao Y, Fang Z, *et al*. Carboxymethyl pachymaran attenuates short-term stress induced depressive behaviours and over-expression of occludin and claudin-2 in the blood–brain-barrier by regulating inflammatory cytokines-JNK/ERK/p38 pathway. Journal of Functional Foods. 2023; 103: 105490.

[24] Wei L, Sun X, Qi X, Zhang Y, Li Y, Xu Y. Dihydromyricetin Ameliorates Cardiac Ischemia/Reperfusion Injury through Sirt3 Activation. BioMed Research International. 2019; 2019: 6803943.

[25] D'Oria R, Schipani R, Leonardini A, Natalicchio A, Perrini S, Cignarelli A, *et al*. The Role of Oxidative Stress in Cardiac Disease: From Physiological Response to Injury Factor. Oxidative Medicine and Cellular Longevity. 2020; 2020: 5732956.